Materials Chemistry and Physics 332 (2025) 130186

Contents lists available at ScienceDirect

Materials Chemistry and Physics

journal homepage: www.elsevier.com/locate/matchemphys

The detection of volatile organic compounds using a CNPs/polypyrrole-based Solid-State sensor operating at room temperature

Lesego Malepe [a], Derek Tantoh Ndinteh [a], Patrick Ndungu [b], Messai Adenew Mamo [a,*]

[a] Department of Chemical Sciences, University of Johannesburg, PO Box 17011, Doornfontein, 2028, Johannesburg, South Africa
[b] Department of Chemistry, University of Pretoria, Private Bag X20, Hatfield, 0028, Pretoria, South Africa

HIGHLIGHTS

- Carbon soot@Polypyrole composite sensor detects volatile organic compounds at room temperature.
- The carbon soot@polypyrrole composite sensor has a fast response and recovery time.
- An *in situ* FTIR-LCR meter was used to study the sensing mechanism for the prepared carbon soot@polypyrrole composite sensors.

GRAPHICAL ABSTRACT

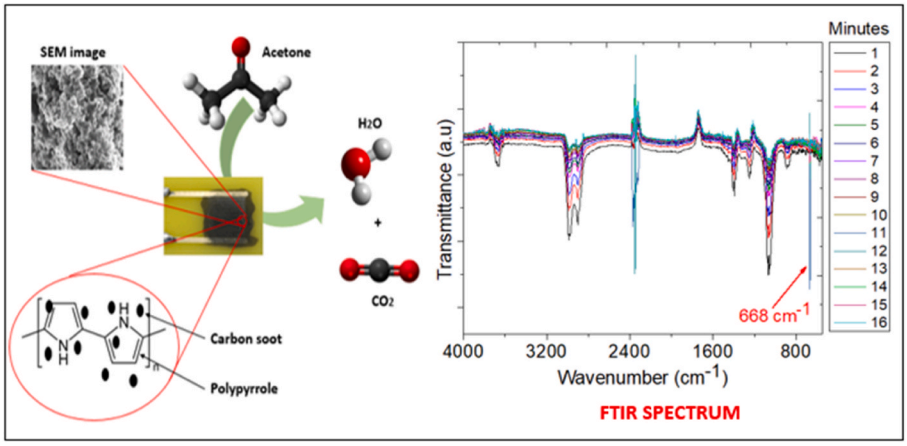

ABSTRACT

In this work, we report the use of carbon nanoparticles (CNPs), commonly as carbon soot, as they are prepared from the pyrolysis of lighthouse candle, polypyrrole (PPy) and carbon nanoparticles@polypyrrole (CNPs@PPy) composite sensors to detect volatile organic compounds at room temperature. Five sensors were fabricated wherein the first sensor was made up of PPy only was named sensor 1, sensor 2 was made up of CNPs only; sensor 3 was made up of a 1:1 mass ratio of CNPs@PPy, sensor 4 was made up of a 2:1 mass ratio of CNPs@PPy, and sensor 5 was fabricated using a 3:1 mass ratio of CNPs@PPy respectively. The sensors were tested dynamically using acetone, 2-propanol, ethanol, and mesitylene vapours. Among all the tested sensors, sensor 5 showed improved sensitivity towards the analytes as compared to sensors; sensor 5 showed higher sensitivity towards acetone vapour than 2-propanol, ethanol, and mesitylene vapours because of a changed amount of CNPs within the composite. The response and recovery times of sensor 5 towards acetone vapour were 72 and 110 s, respectively and a limit of detection (LOD) of 1.212 ppm. Sensor 5 showed a slight increase in acetone vapour as humidity increased. The gas sensing mechanism on sensor 5 was studied using an *in situ* Fourier Transform infrared spectroscopy (FTIR) combined with an LCR meter; basically, the acetone vapour interacts with the solid-state gas sensor supplied with 0.5 V at 25 kHz. The setup confirmed that the acetone completely decomposes into carbon dioxide (CO_2). It was also confirmed that the CO_2 band intensity increases as the exposure time between the acetone vapour and the sensor increases.

* Corresponding author.
E-mail address: messaim@uj.ac.za (M.A. Mamo).

https://doi.org/10.1016/j.matchemphys.2024.130186
Received 21 August 2024; Received in revised form 30 October 2024; Accepted 21 November 2024
Available online 22 November 2024
0254-0584/© 2024 The Authors. Published by Elsevier B.V. This is an open access article under the CC BY-NC-ND license (http://creativecommons.org/licenses/by-nc-nd/4.0/).

1. Introduction

Air pollution caused by evaporated volatile organic compounds (VOCs) may result in human health risks. VOCs are liquid organic compounds that quickly become gaseous at room temperature due to the compounds' low boiling point and high vapour pressure [1]. Examples of VOCs include methanol [2], ethanol [3], propanol [4], toluene [5], acetone [6], chloroform [7], xylene, ethylbenzene, 4-methyl-1-hexene, mesitylene [8] and many more. These VOCs are commonly used in many applications, including cosmetics, pharmaceuticals, agricultural activities, inks, and cleaning detergents. A severe inhalation of these compounds may damage some human organs. Some may result in kidney failure, headache, dizziness, and anaemia [1–8]. Thus, cheap, portable, easy-to-use chemo-resistive gas sensors are needed due to their fast response-recovery times and high sensitivity towards VOCs [9].

Solid-state gas sensors have received significant attention from academics, researchers, and engineers, who have used them to detect or monitor gases and volatile organic compounds in atmospheric environments. These sensors use adsorption/desorption or chemical interactions happening on the surface of a material, commonly such as semiconductor metal oxides. These sensors are also called chemo-resistive gas sensors, as there is a chemical interaction on the material's surface while the change in resistance is monitored [4,9,10]. Semiconductor metal oxides are widely explored in applying gas sensors because of their fast response-recovery times and high sensitivity. unfortunately, they operate at extremely high temperatures ranging from 140 to 400 °C, have poor selectivity towards the targeted VOC, and are easily prone to considerable changes in humidity during measurements [4,10,11]. However, the use of carbon materials such as carbon nanotubes [12], graphene [13] and conductive polymers such as polypyrrole [14], polyaniline [15], and polythiophene [16] are alternative materials as they can operate at lower temperatures and such gas sensors show fast response time. Recently, carbon nanoparticles prepared from pyrolysis of household wax candles received great significant interest in being applied in gas sensors due to their easy preparation (synthesis), ease of great significant interest in being applied in gas sensors due to their easy preparation (synthesis), easy to use, no use of chemicals during preparation, and inexpensive; this material is commonly known as carbon soot [8,17].

Polypyrrole (PPy) is a five-membered ring heterocyclic conductive polymer applied in many applications because of its simple synthesis and low to moderate electrical conductivity. It can be prepared using a simple electrochemical or chemical polymerisation without using any special or unique instrument [14,18,19]. The advantage of applying PPy in gas sensors is their capability to let the sensors operate at lower temperatures [14].

In this work, polypyrrole is mixed with carbon soot (CNPs@PPy composite) used for the detection of VOCs at room temperature, wherein the CNPs are used to improve the reactive oxygen content on the polypyrrole to improve the sensitivity of the VOCs on the prepared sensors as those amounts of reactive oxygen species will be revealed by X-ray photoelectron spectroscopy.

2. Experimental section

2.1. Materials and reagents

Lighthouse white candles were purchased from a local supermarket (shoprite) for the preparation of carbon soot. Mesitylene (99.0 %), ethanol (99.8 %), acetone (99.8), 2-propanol (98.9 %), iron (III) chloride, pyrrole and N–N-dimethylformamide (99.8 %) were purchased from Sigma-Aldrich (Kempton Park, South Africa).

2.2. Preparation of carbon soot

The pyrolysis method is used to prepare carbon nanoparticles (carbon soot). The burning of the lighthouse white candle produced smoke (soot) that was collected using a ceramic cup; the smoke is called carbon soot. The ceramic cup is about 2 cm from the burning candle. After enough accumulation of the candle soot, the ceramic cup was removed from the system and cooled at room temperature. Subsequently, the spatula was used to scrape the soot and store it in a vial.

Table 1
The prepared sensors and their respective mass ratios.

Sensor name	Sensing material	Mass (mg)
Sensor 1	PPy	10
Sensor 2	CNPs	10
Sensor 3	CNPs@PPy	10:10
Sensor 4	CNPs@PPy	20:10
Sensor 5	CNPs@PPy	30:10

2.3. Synthesis of polypyrrole

The synthetic method used to prepare polypyrrole is called chemical polymerisation, as reported by N. Ansari [19]. A 1 M pyrrole solution was prepared by diluting the concentrated pyrrole with deionised water. The calculated molar ratio of the monomer (pyrrole) and an oxidising agent ($FeCl_3$) was 1:2.4. Pyrrole and water were vigorously stirred for about 40 min to obtain a homogeneous mixture. The oxidising agent was added slowly into a stirring pyrrole solution for 30 min at 0–5 °C temperature, maintained by an ice bath. After the oxidising agent was wholly added, the obtained mixture was stirred for 4 h. After the reaction was completed, the polypyrrole was left without stirring at room temperature for 24 h so that the precipitates could settle at the bottom. The precipitates were filtered and washed five times with deionized. The PPy powder was obtained by drying the filtrates for five days at room temperature.

2.4. Gold-plated interdigitated electrode

The sensor was prepared by drop-coating the prepared material onto a gold-plate interdigitated electrode. The electrode was designed to have 0.1 mm width spacing between the gold lines and was counted to be 18 pairs of 7.9 mm long. The electrodes were washed with ethanol and dried at room temperature before use.

2.5. Preparation of polypyrrole, CNPs, and CNPs@PPy sensors

Five sensors were prepared; 10 mg of PPy and CNPs were used to make sensor 1 and sensor 2, respectively. Sensor 3 was made up of a mixture of 10 mg of PPy and 10 mg of CNPs. The mass amount of PPy was kept constant, and the mass amounts of CNPs varied within the composite to prepare sensor 4 and sensor 5 (see Table 1). DMF was the solvent that was used to disperse the sensing materials. Stirred solutions were evenly and gently drop-coated on the gold-plated interdigitated electrodes to fabricate a sensor. The sensors are summarised using the table below.

2.6. Gas sensing setup

Electrical characterisation of the sensors was done using a Keysight E4980A LCR meter connected to a prepared sensor and the computer. The prepared sensor received a voltage of 0.5 alternating current at an ideal relative frequency of 25 kHz. The computer, diaphragm vacuum pump, and LCR metre were connected to a 230 V power source. The prepared sensor was suspended in one neck of the 20L round bottom flask, with four neck openings in the 20L round bottom flask; a similar gas setup was used [20]. The second opening was connected to a diaphragm vacuum pump through 1.5 cm diameter silicone pipes to remove exposed gas inside the flask. The third round bottom flask opening was

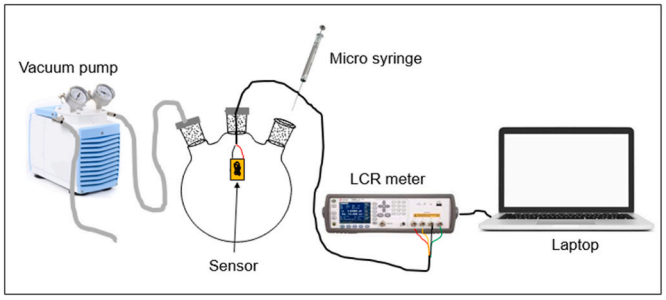

Fig. 1. Gas sensing setup.

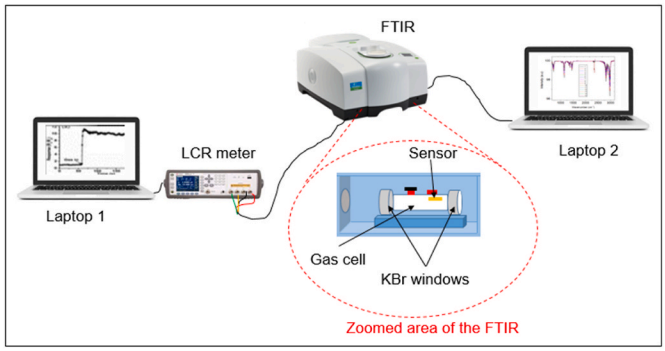

Fig. 2. Schematic illustration of in-situ FTIR coupled with an LCR meter to study the sensing mechanism.

connected to a 4 cm diameter silicone pipe that allowed atmospheric air to enter the flask during the sucking of the presence of the analyte in the round bottom flask. Lastly, the fourth opening was used to introduce our analyte of interest, and the opening was always kept closed after the analyte introduction. The analytes were introduced as liquid inside the flask, and due to the high vapour pressure and low boiling point of the volatile organic compounds, the analytes vaporised easily and interacted with the prepared sensor (see Fig. 1).

The prepared sensors' performance was tested dynamically by exposing each sensor to five different concentrations on every tested VOC. The prepared sensor with the vapour analyte of interest was in contact for 10 min, and the time for removing the exposed gas was 3 min. Then, the sensors kept on running without a vapour analyte for 3 min before another liquid injection was done. The concentration of gas analytes was injected at a time in increasing of volumes 1, 2, 3, 4, and 5 μL. The concentration of the vapour analytes was calculated using the formula labelled equation (1):

$$C = \frac{22.4\rho TVs}{273MV} \times 1000 \quad (1)$$

Where C is the concentration of the vapour analyte, T is the temperature of the environment, Vs is the volume of the liquid analyte injected, ρ is the density of the analyte, M is the molecular weight of the analyte and V is the volume of the round bottom flask [8].

2.7. Sensor response and recovery tests

Response time is when the sensor reaches the maximum response plateau. Recovery time is the time required for the sensor to reach or return to its baseline after the step removal of the gaseous analyte from contact with the sensor. In this study, 90 % of the maximum response was recorded during the analyte's contact with the sensor to record the response time, and 90 % of the sensor's baseline was reached before the recovery time was measured. The relative resistance (ΔR), which is defined as the electrical responses of the prepared sensors to the target gas, was reported and described as

$$\Delta R = R_{gas} - R_{air} \quad (2)$$

where, R_{gas} is the response of a gas analyte and R_{air} is the resistance of the sensor with the reference air [9].

2.8. In Situ FTIR coupled with LCR meter setup and testing

The prepared sensor was positioned on the upper wall of a 110 mL cylindrical glass cell and sealed on both ends with KBr windows. The sensor is electrically connected to an LCR meter. The cell was placed at the centre of the FTIR sample compartment, wherein the IR beam passed through KBr windows that closed the cell. Before the gas analyte was injected into the gas cell, the sensor was run for about 180 min, which is a pre-injection period. A cylindrical cell was filled with about 20 parts per million acetone vapour for the *In Situ* measurement. The LCR meter measured the sensor's electrical response (resistance), and the FTIR spectra were collected every 2 min. The setup is shown in Fig. 2.

2.9. Characterization techniques

Samples were analysed on a JEOL-TEM 2010 (Japan) high-resolution transmission electron microscope (HR-TEM) at an acceleration voltage of 200 kV using the Gatan software. TEM sample preparation, the sample was dispersed in ethanol and DMF (1:2), wherein the mixture was drop coated on Holey carbon-coated copper grids. The Holey carbon-coated copper was allowed to dry with the sample before use. Scanning electron microscopy (SEM) was performed at 30 kV using a FEI Nova Nanolab 600 FEG-SEM. Our samples were sprayed onto SEM pin mount specimens and then carbon coated before analysis. Structural analysis was revealed using powder X-ray diffraction (PXRD), Bruker D2 Phaser using LynxEye detector with radiation of a CuKα at a wavelength of 0.154 nm, and Bruker Senterra laser Raman spectrometer fitted with frequency-doubled Nd-YAG laser with the wavelength of 532 nm. X-ray photoelectron spectroscopy (XPS; XSAM800, Kratos, Manchester, UK) determined the oxidation state and elemental composition. The XPS used Al Kα (1487 eV) radiation as an excitation source, averaging 40 scans, 1 min 17 s, 0.20 eV. Fourier transform infrared spectroscopy (FTIR, PerkinElmer Spectrum 100) was used to determine the sensing mechanism.

3. Results and discussions

3.1. Material Characterisation Characterisation

The yield obtained from the preparation of one candle was found to be 0.314 g. Morphological investigations of carbon soot (CNPs) were examined using transmission electron microscopy (TEM). The TEM images in Fig. 3a–c shows that the CNPs are spherical with an average particle size diameter of 35 nm (see Fig. 3g). As observed in Fig. 3a, the spherical particles are fused, forming chain-like structures. The TEM images of the soot show a high degree of agglomeration. Morphological investigation of PPy, and CNPs@PPy of a mass ratio 3:1 are revealed by scanning electron microscopy (SEM) as presented in Fig. 3d–f. The SEM image shows that the PPy are perfectly rounded particles with an average diameter of 281 nm (see Fig. 3e and **h**). The PPy spherical particles are fused, forming irregular structures (see Fig. 3e). As observed in Fig. 3f, the CNPs spheres are attached to the PPy spheres. The contrast between the CNPs and PPy spheres is particle size, as they are both spheres in appearance.

Powder X-ray diffraction (PXRD) patterns of CNPs, PPy, and CNPs@PPy of mass ratio 3:1 are presented in Fig. 4a–c. CNPs exhibit two broad peaks occurring at $2\theta = 24.8$ and 44° corresponding to (002) and (101), respectively; the crystal planes are in good arrangement with [ICDD: 04-018-7559]. The height of the two peaks characterises the

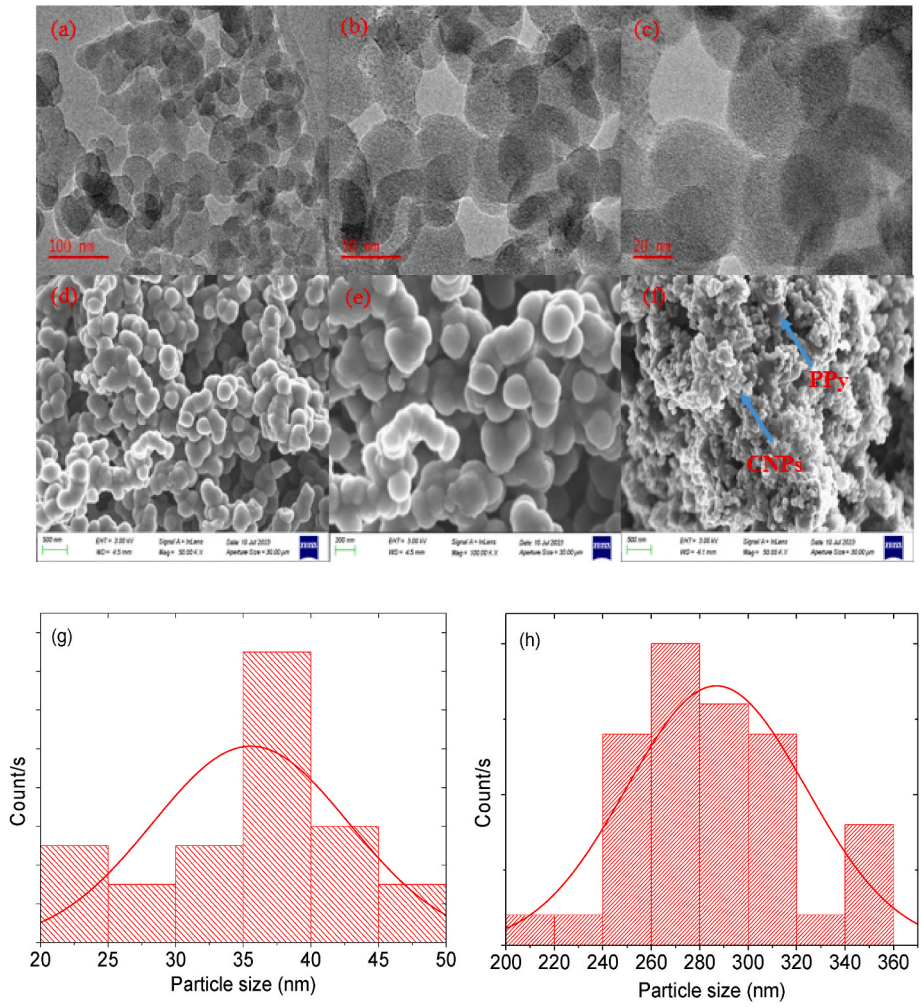

Fig. 3. (a–c) TEM images of CNPs, (d, e) SEM image of PPy, (f) SEM image of CNPs@PPy of a mass ratio 3:1, particle size distribution graphs of (g) CNPs and (h) PPy.

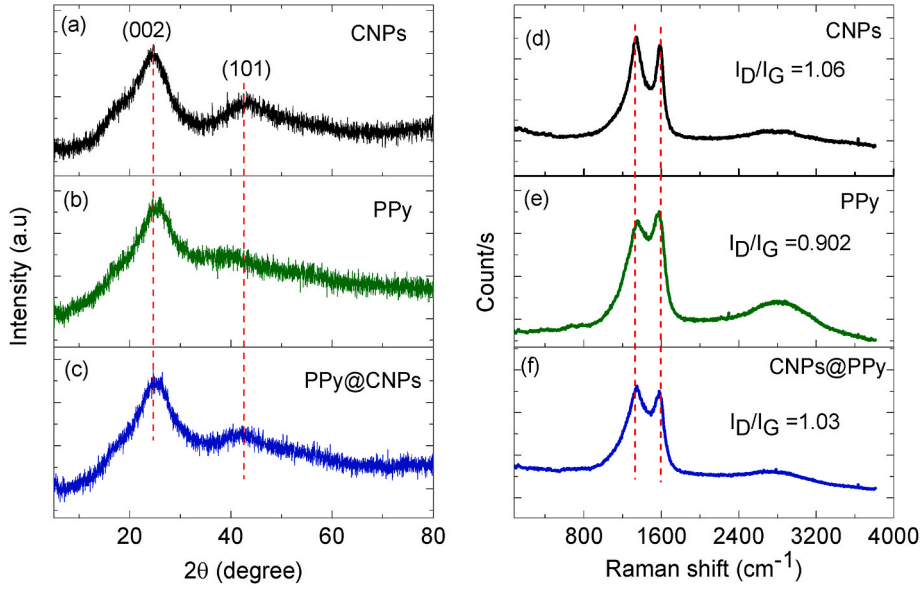

Fig. 4. PXRD pattern of (a) CNPs, (b) PPy, (c) CNPs@PPy, (b) Raman spectra of (d) CNPs, (e) PPy, and (f) CNPs@PPy.

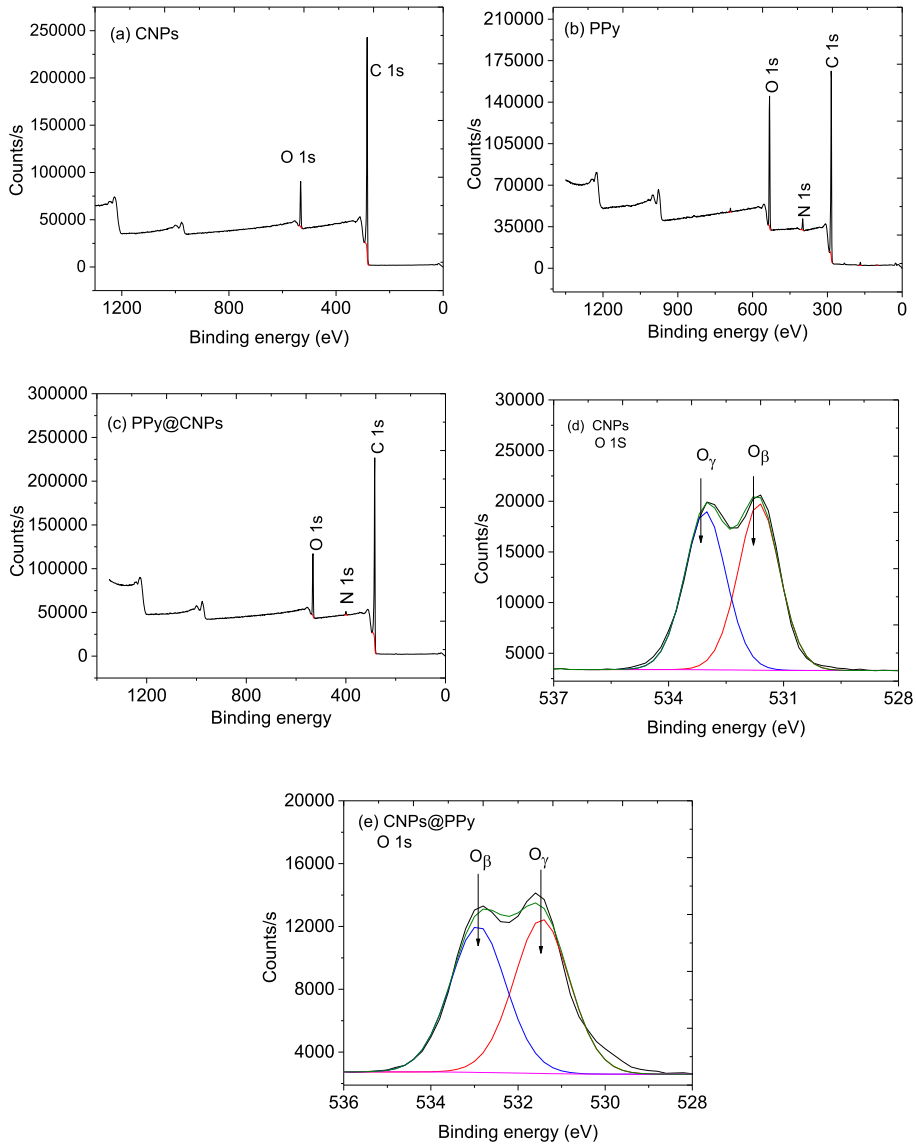

Fig. 5. XPS analysis, (a) CNPs survey, (b) PPy survey, (c) CNPs@PPy survey, O 1s of (d) CNPs, (e) CNPs@PPy of 3:1 mass ratio.

graphitic carbon of the CNPs. The peak positioned at $2\theta = 24.8$ indicates the successful synthesis of PPy similar findings were reported by J. Wang et al. [21]. In addition, both the CNPs, and PPy are amorphous. CNPs have (101) and (002) crystal planes, and while PPy has only (002), meanwhile, the CNPs@PPy composite show both (101), and (002); in addition, there is no new peak formed. Fig. 4d–f presents Raman spectra of CNPs, PPy, and CNPs@PPy of the mass ratio 3:1; all the materials show two broad peaks occurring at 1350 and 1555 cm^{-1} designated to D and G bands. Raman spectroscopy was used to study the D and G bands intensities (I_D/I_G) ratio of the PPy, CNPs, and CNPs@PPy composite. Perumbilaval et al. [22] reported that the I_D/I_G is affected by the oxygen species present in the material, where the authors discussed that the D

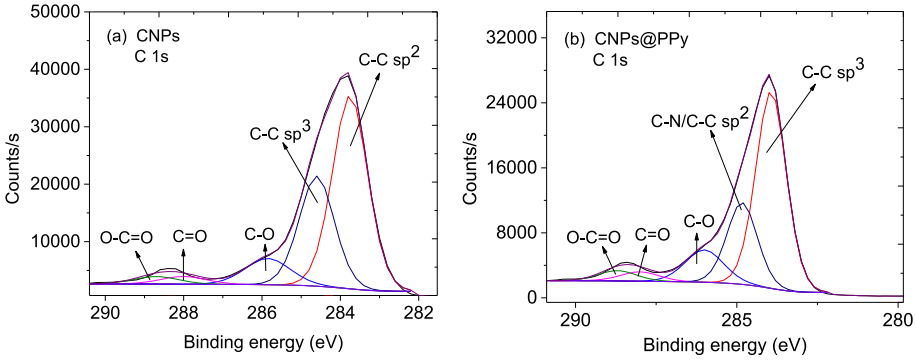

Fig. 6. C 1s scan of (a) CNPs, and (b) CNPs@PPy.

Table 2
The calculated percentage of oxygen species in the materials.

CNPs Peak positioned (eV)	Atomic % of oxygen	CNPs@PPy Peak positioned (eV)	Atomic % of oxygen
O_β →42.7	57.3	O_β →531.7	52.4
O_γ → 57.3	42.7	O_γ → 533.1	47.6

and G intensity ratio of graphene is increased from 0.7 to 1.03 for graphene oxide because of the oxygen species in the graphene oxide. The I_D/I_G ratio of PPy was 0.902, CNPs was 1.06, and CNPs@PPy composite was 1.03; this change in I_D/I_G might be due to the existence of oxygen reactive species on CNPs are the main reason for the I_D/I_G of CNPs@PPy composite to increase as compared to that of PPy (see Fig. 4d–f).

The XPS analysis was conducted to reveal the chemical composition, the type of oxygen species, and the bonding nature in the CNPs, PPy, and CNPs@PPy composite. The XPS survey of CNPs shows the presence of carbon (C) and oxygen (O) only (see Fig. 5a). The XPS survey indicates

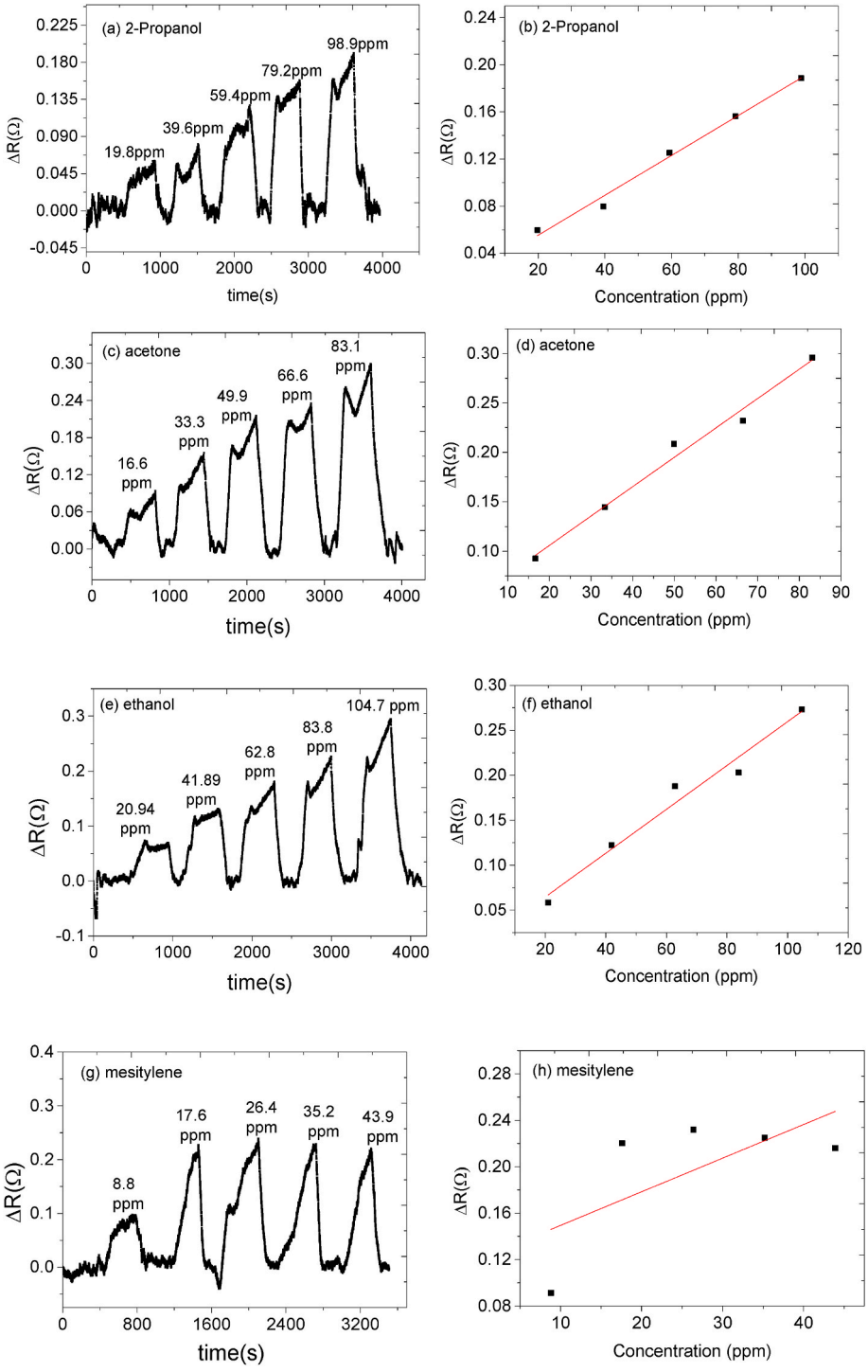

Fig. 7. Relative electrical resistive response curves of (a) 2-propanol, (c) acetone (e) ethanol, (g) mesitylene vapours on sensor 4 and their respective sensitivity calibration curve (b) 2-propanol, (d) acetone (f) ethanol (h) mesitylene vapours.

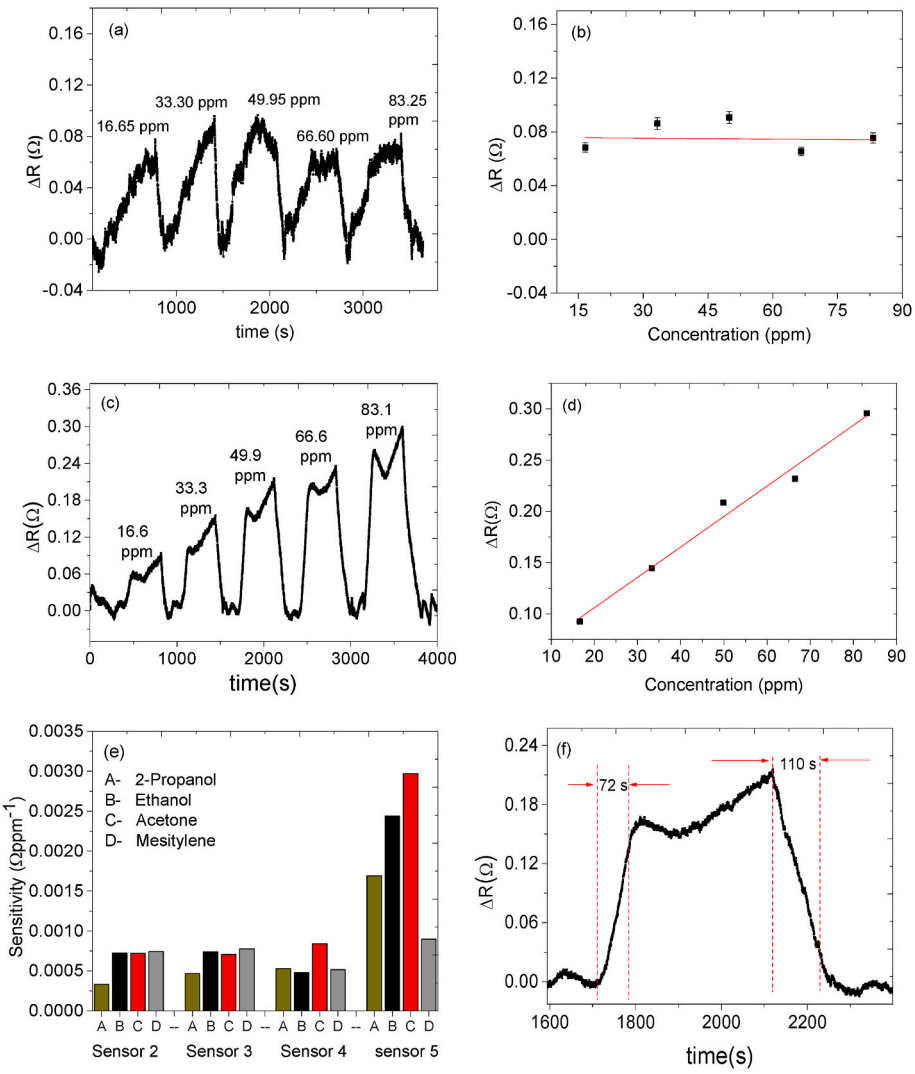

Fig. 8. (a) Relative resistance response curve of sensor 1 on acetone vapour, (b) its sensitivity calibration curve, (c) relative resistance response curve of sensor 5 on acetone vapour and (d) its sensitivity calibration curve, (e) sensitivity bar graph, and (f) relative response-recovery curve of sensor 4 on acetone.

that the PPy and CNPs@PPy are composed of carbon (C), nitrogen (N), and oxygen (O), as presented in Fig. 5b and c. The XPS O 1s spectra of CNPs have O_β and O_γ positioned at 531.8 eV and 533.1 eV, respectively. The oxygen species labelled O_β represents the surface adsorbed oxygen, while the oxygen species O_γ represents the adsorbed OH on the material's surface [23]. The C 1s scan of CNPs and CNPs@PPy is deconvoluted into peaks at 283.8 eV, 284.6 eV, 286 eV, 287.8 eV, 288.8 eV assigned for C–C sp^2, C–C sp^3, hydroxyl group (C–O), carbonyl group (C═O), and carboxyl group (O–C═O), respectively [20] as presented in Fig. 6a), but the C–C sp^3 overlaps with C–N at 284.6 eV for PPy (see Fig. 6b). The Gaussian function fitted the two oxygen species named Oβ and Oγ of the O 1s of CNPs and CNPs@PPy composite. The fitted area of oxygen species is expressed in percentages as summarised in Table 2. CNPs@PPy composite have oxygen species, O_β and O_γ, which play a crucial role in VOC sensing. The 3:1 mass ratio of CNPs@PPy composite has oxygen species, which could be why the composite responds better than pure PPy.

3.2. Gas sensing application

3.2.1. Gas responses and sensitivity

In this gas sensing application, sensing materials that are used in detecting VOCs (namely: 2-propanol, acetone, ethanol, and mesitylene vapours) are PPy, CNPs, and CNPs@PPy hybrids. The amount of PPy within the CNPs@PPy composite was kept constant while the mass of CNPs was varied to prepare sensor 3, sensor 4, and sensor 5. Sensor 2 is made up of CNPs only; sensor 3 is made up of a 1:1 mass ratio of CNPs@PPy; sensor 4 is made up of a 2:1 mass ratio of CNPs@PPy, and sensor 5 is fabricated using a 3:1 mass ratio of CNPs@PPy respectively. All the prepared solid-state gas sensors' performances were tested at room temperature.

The PPy based sensor 1 was tested separately on the VOCs mentioned above, and no response was observed (see sensing result in Fig. S1) [24]. Sensor 2 showed some responses towards 2-propanol, ethanol, acetone, and mesitylene; however, it has a low signal-to-noise ratio (see Fig. 8a and b) and Fig. S2). Incorporating PPy with CNPs (sensor 2 and sensor 3) showed a higher signal-to-noise ratio than sensor 2. All the responded sensors showed increased resistance during the sensor's interaction with the analyte vapour except for the mesitylene vapour. When the analyte was removed from the chamber, the sensor's resistance decreased and returned to the baseline (See Fig. 7). Furthermore, the sensitivity of the three sensors towards the tested analyte vapours (sensor 2, sensor 3, and sensor 4) was almost equal for all the analytes. However, sensor 5 showed high sensitivity on the analytes compared to sensor 2, sensor 3, and sensor 4. Sensor 5 shows an increase in gas response as the concentration of gases increases (see Fig. 8c) and the linearity was observed

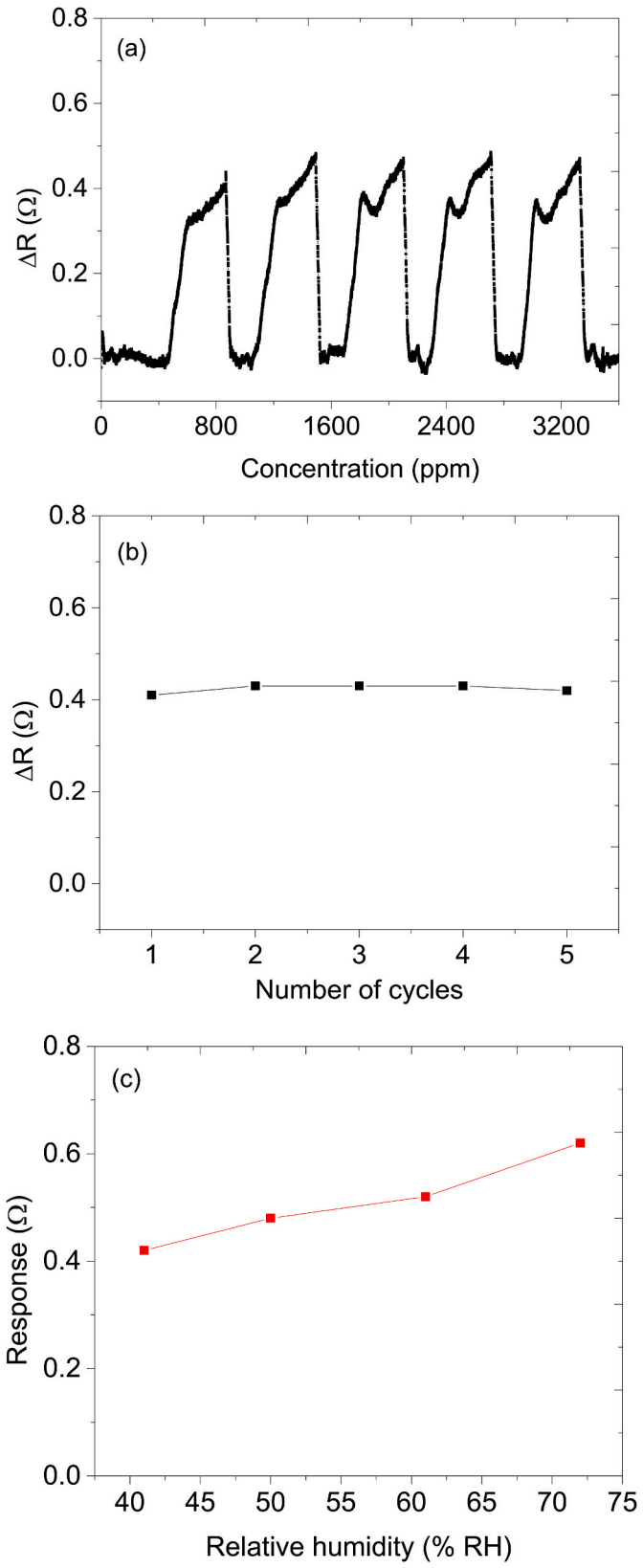

Fig. 9. (a) Repeatability acetone vapour electrical resistance response curve, (b) its amplitude profile and (c) response-relative humidity graph.

Table 3
Comparison of various materials reported of acetone vapour gas sensors.

Sensing materials	Acetone (ppm)	Res/rec time (s)	Response (ohms)	Temp (°C)	Ref
SnO_2/PPy	100	–	1.1	Room	[27]
PPy/MnO_2	30	–	1	Room	[28]
PPy/Zn_2SnO_4	1	26/24	0.9	Room	[29]
QDs/PPy (1:10)	5	–	4	Room	[30]
CNPs@PPy (3:1)	11.5	42/58	0.2	Room	**This work**

(–) not recorded.

as shown in Fig. 8d. Thus, among all the fabricated sensors, sensor 5 was considered the best as it showed approximately 2.4 times more sensitivity than sensors 1, 2, and 3 towards the analytes vapour (see Fig. 8e). Sensor 5 is highly sensitive to acetone vapour (0.00297 Ω ppm^{-1}) and less sensitive to ethanol (0.00244 Ω ppm^{-1}), 2-propanol (0.00169 Ω ppm^{-1}), and mesitylene (0.00029 Ω ppm^{-1}) vapours. The response and recovery time for acetone vapour of sensor 5 were 72 and 110 s, respectively (see Fig. 8f).

3.2.2. *Repeatability and humidity evaluations*

The ability of the gas sensors to regenerate themselves and reproduce the same result over time is very important. Acetone concentration (99.01 ppm) was injected into a vacuum chamber in contact with sensor 5 for five cycles to investigate the repeatability. It was found that the results obtained were almost the same, with a maximum amplitude value of 0.42 Ω, as presented in Fig. 9. The five maximum electrical responses of the acetone vapour were found to be 0.418 Ω, 0.428 Ω, 0.420 Ω, 0.420 Ω, and 0.419 Ω. The average electrical response was 0.421 ± 0.00358 Ω, showing that the sensor's response was almost the same over five cycles. This indicates that the sensor is stable and reads the same value when it is repeatedly exposed to the same concentration. Sensor 5 showed a fast response to acetone vapour, and it recovered well during the removal of the gases formed during sensing in the presence of atmospheric air containing oxygen molecules. Sensor 5 showed good regeneratability for the detection of acetone vapour.

According to the literature reports from the gas sensors under study, humidity can generally impact how well the sensors work [8,25]. Hence, the humidity of sensor 5 on acetone vapour was studied from the humidity range of 41–73 % relative humidity (% RH). Sensor 5 was subjected to identical concentrations (99.01 ppm) of acetone vapour at varying humidities in order to examine their respective responses. The maximum relative response of 99.01 ppm acetone vapour using sensor 5 at relative humidities 41 %, 49 %, 61 % and 73 % were 0.42 Ω, 0.48 Ω, 0.52 Ω, and 0.62 Ω, respectively (see Fig. 9c). It has been noted that there is a slight increase in sensor responses as humidity rises. This observation may be due to water molecules that have adsorbed on the surface of the sensing materials, slightly altering the response.

3.2.3. *Limit of detection*

It is very important to know the least possible concentration that can be detected by the sensor. The lowest possible concentration to be detected in gas sensors is important to be known, commonly known as the Limit of detection (LOD). LOD The calibration curve between the acetone vapour and electrical response gives a correlation coefficient (R^2) of 0.99 and a slope of 0.00297 Ω ppm^{-1}. The LOD = 3 × RMS/slope [26], wherein the RMS is the standard deviation with a value of 0.00012, and the LOD is 1.212 ppm. CNPs@PPy 3:1 mass ratio (sensor 5) can detect toluene vapour even at the lowest concentration (sub-ppm). Unfortunately, our gas sensing system cannot test the fabricated sensors at the lowest possible concentration (1.212 ppm) that the sensor can detect, but the theoretical calculation indicates that the sensor can detect as low as 1.212 ppm.

Our work was compared with previously reported polypyrrole-based sensors in detecting acetone vapour operating at room temperature (see

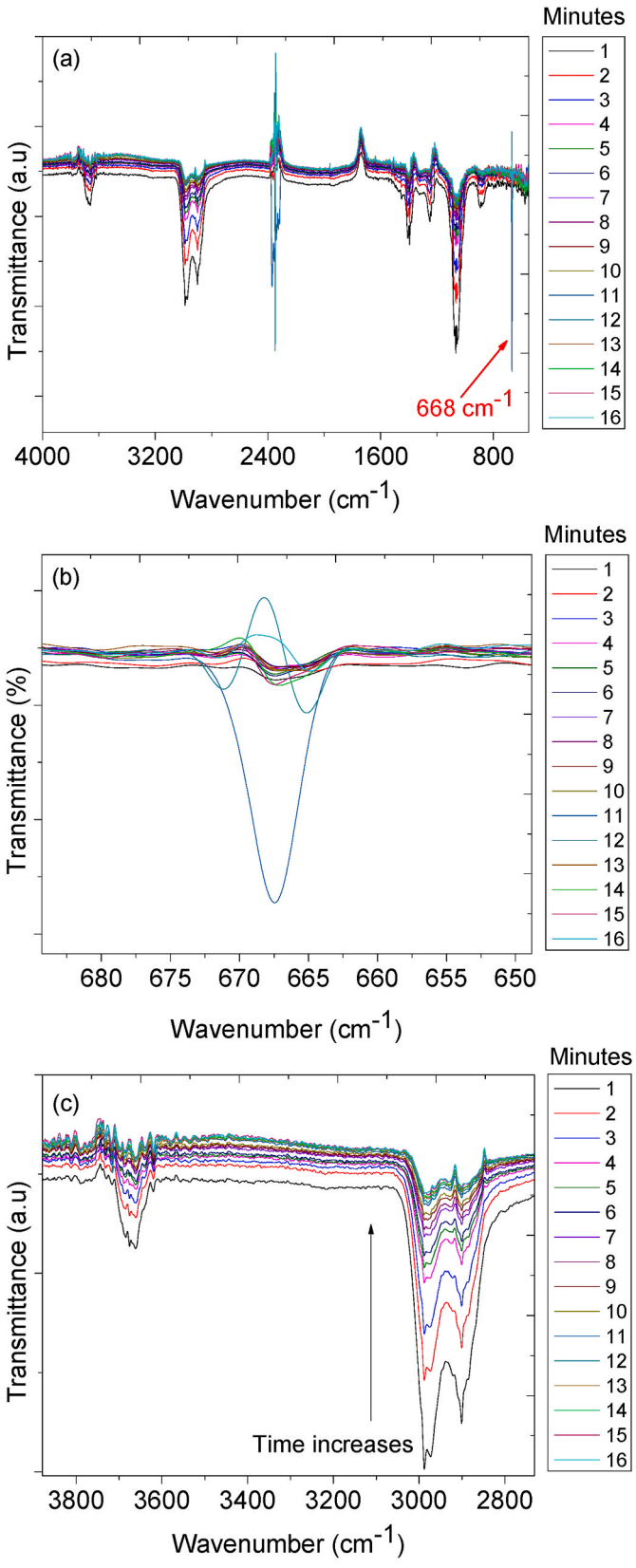

Fig. 10. The LCR meter coupled with FTIR spectra, (a) full FTIR spectrum of the acetone vapour, (b) zoomed FTIR spectrum showing 668^{-1} band, and (c) 3800-2800 cm^{-1}.

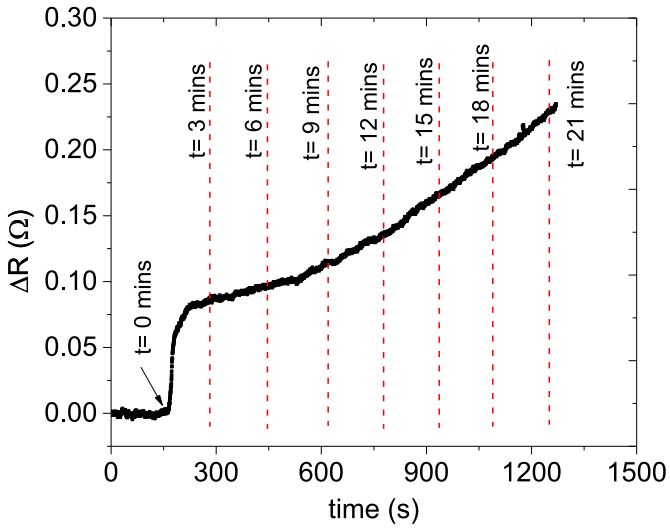

Fig. 11. The LCR meter coupled with FTIR spectra the *in situ* the electrical response of the sensor.

Table 3). Our work showed a reasonable response and recovery time.

3.2.4. Gas sensing mechanism

(a) General sensing mechanism

It is believed that the sensing mechanism of polymer-based is different from that of semiconductor metal oxides. The SMOs usually undergo a total deep oxidation of analyte to produce CO_2 and H_2O gases. In the case of polymers such as PPy, electrostatic interactions and Lewis acid-base are used between the sensing material and the analyte. In addition, polarisation interactions also apply, wherein the more polar gaseous analytes have a higher affinity for interaction. Lewis base-acid interactions occur when the vapour analyte or the polymer has lone pairs of electrons [31]. The weak bond between the analyte and the polymer is created by donating or accepting a pair of electrons [32]. On the other hand, different sensing mechanisms could be applied by adsorbing vapour molecules on the surface of the polymer, and the polymer starts to swell as its volume increases. The process results in a change in the conductivity or resistivity of the sensing material. The accepted sensing mechanism of carbon-based materials is charge transfer between the sensing material and the vapour analyte [33]. CNPs also use an adsorption-desorption mechanism wherein the adsorbed vapour decomposes into CO_2 and H_2O gases [17].

(b) In-situ FTIR-online LCR meter measurement

Understanding the sensing mechanism of CNPs@PPy on acetone vapour detection was a crucial step in sensor fabrication. During the measurement, the LCR measures the electrical performance of the sensors during the sensor-analyte interactions; at the same time, FTIR instruments measure the gas analyte in the gas cell. The sensor's surface interaction and the analyte molecules are expected to produce new molecules, which helps us understand the sensing mechanism. For this particular experiment, we used acetone as the analyte gas. The FTIR spectra were taken every minute for 21 min (here we presented the first 16 min spectra only), while the electrical response was recorded continuously for 21 min. This experiment was designed so that the IR bands could monitor the gas samples and the LCR meter to measure the change in resistance of the sensor *in situ* concurrently with the FTIR instrument. The FTIR band of interest, at 668 cm^{-1}, was due to carbon dioxide (see Fig. 10a–c). There is an increase in CO_2 IR band at 668 cm^{-1} (see Fig. 10b). The decomposition of acetone is further proved by

studying the C–H stretching band intensity occurring at 2900-3100 cm^{-1} decreases as the time of exposure with the sensor increases; the acetone is breaking down into CO_2 gas and H_2O. This could result from the presence of high content of CNPs in sensor 5, which could be why the adsorption-desorption mechanism of polymer/carbon material composite sensor dominates. On the other hand, the results from the LCR meter show that the sensor resistance was increased as time elapsed (See Fig. 11), which showed that there was a reaction on the surface of the sensing material and the intensity of the analyte continuously decreased, which shows the acetone decomposed over the surface of the sensing material and produced CO_2 gas. The increases in the CO_2 IR band intensity confirmed the continued production of CO_2 gas.

4. Conclusion

In summary, the prepared CNPs, PPy, and CNPs@PPy were characterised using SEM, TEM, XPS, and Raman spectroscopy. It was found that an increased amount of CNPs within the composite at 3:1 mass ratio (CNPs@PPy) improved the sensing of VOCs as compared to pure CNPs sensor, 1:1 mass ratio of CNPs@PPy and 2:1 mass ratio of CNPs@PPy, especially when looking at acetone vapour as it showed high sensitivity among other tested vapour analytes. However, the sensor showed poor selectivity towards acetone vapour. The aimed of the work was reached as it was to investigate the effect of sensitivity of the sensors towards the analytes as the carbon soot weight within the CNPs@PPy composite changes. And the highly analyte was found to be acetone and further studied its sensing mechanism using an in-situ FTIR coupled with LCR meter. Sensor 5 was found to have fast response and recovery times of 72 s and 110 s, and the LOD is 1.212 ppm towards the acetone vapour. The sensing mechanism of sensor 5 with acetone was deployed, and it was observed that acetone vapour breaks down into carbon dioxide and water as desorbed products.

CRediT authorship contribution statement

Lesego Malepe: Writing – original draft, Visualization, Methodology, Investigation, Formal analysis, Data curation. **Derek Tantoh Ndinteh:** Writing – review & editing, Visualization, Validation, Supervision, Resources, Investigation, Formal analysis. **Patrick Ndungu:** Writing – review & editing, Visualization, Validation, Supervision, Investigation, Formal analysis, Data curation. **Messai Adenew Mamo:** Writing – review & editing, Visualization, Validation, Supervision, Resources, Project administration, Methodology, Investigation, Funding acquisition, Formal analysis, Data curation, Conceptualization.

Declaration of competing interest

We declare any conflict of interest in the manuscript submitted under the title of “The detection of volatile organic compounds using a CNPs/polypyrrole-based solid-state sensor operating at room temperature” in any form.

Acknowledgements

Lesego Malepe thanks the University of Johannesburg for financial assistance. All authors acknowledge the University of Johannesburg for financial assistance.

Appendix B. Supplementary data

Supplementary data to this article can be found online at https://doi.org/10.1016/j.matchemphys.2024.130186.

Appendix A. Supplementary data

The following are the Supplementary data to this article.

Data availability

Data will be made available on request.

References

[1] A. Mirzaei, S.G. Leonardi, G. Neri, Detection of hazardous volatile organic compounds (VOCs) by metal oxide nanostructures-based gas sensors, Ceram. Int. 42 (2016) 15119.
[2] Y. Li, D. Denga, X. Xinga, N. Chenb, N. Liua, X. Xiaoa, Y. Wang, A high-performance methanol gas sensor based on palladium-platinum-In_2O_3 composited nanocrystalline SnO_2, Sens. Actuators, B 237 (2016) 133–141.
[3] T. Tharsika, M. Thanihaichelvan, A.S.M.A. Haseeb, S.A. Akbar, Highly sensitive and selective ethanol sensor based on ZnO nanorod on SnO_2 thin film fabricated by spray pyrolysis, Front. Mater. 6 (2019) 122.
[4] T.P. Mokoena, K.T. Hillie, H.C. Swart, N. Leshabane, J. Tshilongo, D.E. Motaung, Fabrication of a propanol gas sensor using p-type nickel oxide nanostructures: the effect of ramping rate towards luminescence and gas sensing characteristics, Material chemistry and physics 253 (2020) 123316.
[5] S.P. Subin David, S. Veeralakshmi, J. Sandhya, S. Nehru, S. Kalaiselvam, Room temperature operatable high sensitive toluene gas sensor using chemiresistive Ag/Bi_2O_3 nanocomposite, Sens. Actuators, B 320 (2020) 128410.
[6] C. Li, P.G. Choi, K. Kim, Y. Masuda, High performance acetone gas sensor based on ultrathin porous NiO nanosheets, Sens. Actuators, B 367 (2022) 132143.
[7] D.S. Chandrasakaran, I. Nainggolan, N. Derman, T. Ikhsan, Chloroform gas sensor based on chitosan biopolymer, Appl. Mech. Mater. 679 (2014) 45–49.
[8] L. Malepe, D. Ndinteh, M.A. Mamo, The effect of measurement parameters on the performance of the sensors in the detection of organic compound vapours, Chemical Physics Impact 4 (2022) 100068.
[9] A. Dey, Semiconductor metal oxide gas sensors: a review, Mater. Sci. Eng. B 229 (2018) 206.
[10] Y. Tan, J. Zhang, Highly sensitive ethanol gas sensors based on Co-doped SnO_2 nanobelts and pure SnO_2 nanobelts, Phys. E Low-dimens. Syst. Nanostruct. 147 (2023) 115604.
[11] Z. Yuan, J. Li, F. Meng, High response n-propanol sensor based on co-modified ZnO nanorods, J. Alloys Compd. 910 (2022) 164971.
[12] L.A. Panes-Ruiz, M. Shaygan, Y. Fu, Y. Liu, V. Khavrus, S. Oswald, T. Gemming, T. Baraban, V. Bezugly, G. Cuniberti, Toward highly sensitive and energy efficient ammonia gas detection with modified single-walled carbon nanotubes at room temperature, ACS Sens. 3 (2018) 79–86.
[13] H. Fei, G. Wu, W. Cheng, W. Yan, H. Xu, D. Zhang, Y. Zhao, Y. Chen, L. Zhang, C. Coileain, Enhanced NO_2 sensing at room temperature with graphene via monodisperse polystyrene bead decoration, ACS Omega 4 (2019) 3812–3819.
[14] M. Šetka, J. Drbohlavová, J. Hubálek, Nanostructured polypyrrole-based ammonia and volatile organic compound sensors, Sensors 17 (2017) 562.
[15] D. Maity, R.T.R. Kumar, Polyaniline anchored MWCNTs on fabric for high performance wearable ammonia sensor, ACS Sens. 3 (2018) 1822–1830.
[16] A. Husain, S. Ahmad, M.U. Shariq, M.M.A. Khan, Ultra-sensitive, highly selective and completely reversible ammonia sensor based on polythiophene/SWCNT nanocomposite, Materialia. 10 (2020) 100704.
[17] L. Malepe, P. Ndungu, D.T. Ndinteh, M.A. Mamo, Nickel oxide-carbon soot-cellulose acetate nanocomposite for the detection of mesitylene vapour: investigating the sensing mechanism using an LCR meter coupled to an FTIR spectrometer, Nanomaterials 12 (2022) 727.
[18] H.K. Chitte, N.V. Bhat, V.E. Walunj, G.N. Shinde, Synthesis of polypyrrole using ferric chloride ($FeCl_3$) as oxidant together with some dopants for use in gas sensors, J. Sens. Technol. 1 (2011) 10.
[19] R. Ansari, Polypyrrole conducting electroactive polymers: synthesis and stability studies, E-J Chem. 3 (2006) 186.
[20] C.K. Gaddam, R.L. Vander Wal, Physical and chemical characterisation of SIDI engine particulates, Combust. Flame 160 (2013) 2517–2528.
[21] J. Wang, B. Wei, F. Kang, Facile synthesis of hierarchical conducting polypyrrole nanostructures via a reactive template of MnO_2 and their application in supercapacitors, RSC Adv. 4 (2014) 199–202.
[22] S. Perumbilavil, P. Sankar, T.P. Rose, R. Philip, White light Z-scan measurements of ultrafast optical nonlinearity in reduced graphene oxide nanosheets in the 400–700 nm region, Appl. Phys. Lett. 107 (2015) 051104.
[23] H. Guo, Z. Zhang, Z. Jiang, M. Chen, H. Einaga, W. Shangguan, Catalytic activity of porous manganese oxides for benzene oxidation improved via citric acid solution combustion synthesis, J. Environ. Sci. 98 (2020) 196–204.
[24] K. Namsheer, S.R. Chandra, Conducting polymers: a comprehensive review on recent advances in synthesis, properties, and applications, RSC Adv. 11 (2021) 5659–5697.
[25] J. Wang, P. Yang, X. Wei, High-performance, room-temperature, and no-humidity-impact ammonia sensor based on heterogeneous nickel oxide and zinc oxide nanocrystals, ACS Appl. Mater. Interfaces 7 (2015) 3816–3824.
[26] O. Leenarrts, B. Partoens, F.M. Peeters, Adsorption of H_2O, NH_3, CO, NO_2, and NO on graphene: a first-principles study, Phys. Rev. B Condens. Matter 77 (2008) 125416.
[27] S. Bagchi, C. Ghanshyam, Understanding the gas sensing properties of polypyrrole coated tin oxide nanofiber mats, J. Phys. D Appl. Phys. 50 (2017) 10.
[28] K. Malook, H. Khan, M. Shah, H. Ihsan Ul, Highly selective and sensitive response of Polypyrrole-MnO_2 based composites towards ammonia gas, Polym. Compos. 40 (2019) 1676–1683.

[29] D. Zhang, Z. Wu, X. Zong, Y. Zhang, Fabrication of polypyrrole/Zn2SnO4 nanofilm for ultra-highly sensitive ammonia sensing application, Sens. Actuators B Chem. 274 (2018) 575–586.
[30] M. Šetka, F.A. Bahos, O. Chmela, D. Matatagui, I. Gràcia, J. Drbohlavová, S. Vallejos, Cadmium telluride/polypyrrole nanocomposite based Love wave sensors highly sensitive to acetone at room temperature, Sens. Actuators B Chem. 321 (2020) 128573.
[31] C.K. Tan, D.J. Blackwood, Interactions between polyaniline and methanol vapour, Sens. Actuators, B 71 (2000) 184.
[32] K. Hirayama, Y. Sakai, K. Kameoka, K. Noda, R. Naganawa, Preparation of a sensor device with specific recognition sites for acetaldehyde by molecular imprinting technique, Sens. Actuators, B 86 (2002) 20–25.
[33] J. Zhang, A. Boyd, A. Tselev, M. Paranjape, P. Barbara, Mechanism of NO_2 detection in carbon nanotube field effect transistor chemical sensors, Appl. Phys. Lett. 88 (2006) 123112.
[1] G.K. Gowtham, G. Thejas Urs, H. Somashekarappa, R. Somashekar, Preparation, and crystal structure of carbon soot: a new approach, AIP Conf. Proc. 2265 (2020) 030164.